Bound-Bound State Quantum Wave Packet Dynamics in the Intermediate Coupling Range: The $A\,^1\Sigma_u^+$ (0_u^+) and $b\,^3\Pi_u$ (0_u^+) System in Rb_2

Bo Zhang and Niklas Gador

Royal Institute of Technology, AlbaNova University Center, Department of Physics, SE-106 91 Stockholm, Sweden

Tony Hansson*

Stockholm University, AlbaNova University Center, Department of Physics, SE-106 91 Stockholm, Sweden

(Received 24 June 2003; published 24 October 2003)

The real-time quantum dynamics of a wave packet confined to two coupled bound states at intermediate interaction strength is probed by experiment and calculations on the $A\,^1\Sigma_u^+ \sim b\,^3\Pi_u$ system in Rb_2 molecules. The general dynamics consists of rapid spreading out over the whole phase space. Particular conditions exist, however, under which the initial wave packet motion separates into two mesobatic trajectories with distinct frequencies. These diabatic or adiabatic hybrid trajectories are analogous to those responsible for longevity resonances in bound-unbound systems.

DOI: 10.1103/PhysRevLett.91.173006 PACS numbers: 33.50.–j, 34.30.+h, 82.20.Gk, 82.53.–k

A quantum system traversing a state level crossing is a general phenomenon occurring in essentially all fields of natural science, for instance, in neutrino flavor conversion [1], nuclear reactions [2], chemistry in interstellar space [3], and vision and other biological light harvesting processes [4]. Depending on the relation of the time scales for mixing of the coupled states and traversal of the crossing region, conveniently parametrized in terms of $\gamma \equiv V/\nu_u^{ad}$, where V is the coupling between the two diabatic states and ν_u^{ad} the vibrational frequency of the upper adiabatic state, the crossing can be classified as either adiabatic for $\gamma \to \infty$ or diabatic in the opposite limit $\gamma \to 0$. In either case the quantum state representation is clear with well-defined basis sets and small coupling matrix elements between the corresponding states, and the crossing events are well described by perturbative methods. In the intermediate $\gamma \approx 1$ range, however, neither limiting description is adequate and the primary crossing process may be viewed as a strong mixture of the two asymptotic cases [5,6].

Within the particular framework of molecules the intermediate coupling situation represents the worst instance of breakdown of the Born-Oppenheimer approximation to decouple the motion of electrons and atomic nuclei. It thus paves the way for strong dynamical, i.e., nonadiabatic, effects on the electronic state evolution and, consequently, the molecule's chemical properties. These dynamical effects have been little explored by direct experiments, however. Stolow and co-workers [7,8] performed the only real-time studies of a system in this coupling strength range, the bound-unbound state interaction in predissociation of the IBr $(B\,^3\Pi_{0^+})$ state. Most notably, they found at certain excitation wavelengths pronounced long-lived resonances with a distinct vibrational frequency, qualitatively explained as arising from interference between wave packets traveling along adiabatic and diabatic trajectories analogous to adiabatic trapping in strong-field photodissociation. Other authors interpreted results from similar systems in terms of interference between adiabatic [9] or diabatic wave packets [10,11]. In the latter case the formal similarity to Stückelberg oscillations in particle scattering probabilities was pointed out [10]. In a semiclassical path integral model, finally, the resonances occur for any coupling strength whenever an adiabatic bound level and a diabatic one are degenerate [12] which for IBr was found to be a propensity rule rather than a strict one [13].

The various views on the nature of these wave packet interferences are not obviously commensurate. To throw light on the problem from a new angle we discuss in this Letter real-time measurements and calculations on the quantum wave packet dynamics in a molecular system of two bound states in the intermediate coupling case. Expectedly, we find the general dynamics to consist of rapid spreading out over the available classical phase space. There exist particular resonancelike conditions, however, under which the wave packet motion separates into two distinct, noninteracting trajectories, each analogous to the trapped wave packet motion in predissociation. In view of the inadequacy of the diabatic/adiabatic classification at intermediate coupling strength we prefer to regard this as a state of motion in its own named mesobatic.

The particular system we studied is shown in Fig. 1. In the Hund's case *a* representation it consists of the $A\,^1\Sigma_u^+$ and $b\,^3\Pi_u$ states crossing at an internuclear separation of 5.1 Å and going to the $5s + 5p$ separated-atoms limit. As in the other homonuclear diatomic alkali molecules these states may couple by spin-orbit (SO) interaction with respect to which they are diabatic. Because of the $\Delta\Omega = 0$ selection rule for the interaction only the $\Omega = 0$ component is directly involved. Thus, diagonalizing the SO interaction matrix one obtains two Hund's case *c* relativistic adiabatic states of 0_u^+ symmetry

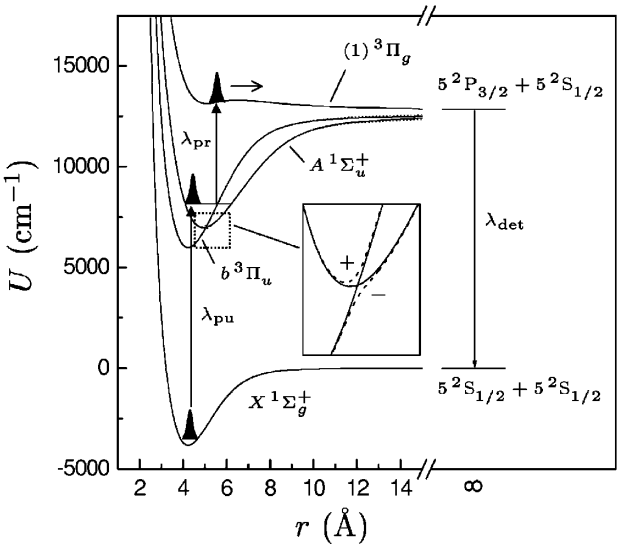

FIG. 1. Potential energy curves of Rb_2 [14] and the pump-probe measurement scheme. The pump wavelength $\lambda_{pu} =$ 865–942 nm and the probe wavelength $\lambda_{pr} = 1700$ nm. Atomic $D2$ line emission at $\lambda_{det} = 780$ nm is detected. Inset: magnified view of the level crossing region and labeling of the adiabatic curves.

correlating to the $5\,^2P_{1/2,3/2} + 5\,^2S_{1/2}$ atomic limits. The SO coupling matrix element at the curve crossing may be estimated to $V_{Ab}^{\times} \approx 75\ \mathrm{cm}^{-1}$ [15] which corresponds to $\gamma_{Ab} = 1.4$. This is in the intermediate coupling range and as neither the adiabatic nor diabatic picture is adequate we arbitrarily choose in the following to use mostly the relativistic diabatic $\{A, b\}$ labeling of the states. Whenever we refer to the relativistic adiabatic representation, $\{+, -\}$ notate the upper and lower 0_u^+ states, respectively.

To bring out the quantum wave packet dynamics in this fully coupled bound-bound state system we apply the pump-probe scheme sketched in Fig. 1. A pump pulse launches a wave packet at the inner turning point of the A state. This wave packet then moves towards the crossing region where it may undergo intersystem crossing to the b state. After some time delay Δt the probe pulse interrogates the wave function at the outer turning point of the b state by projecting part of it onto the unbound $(1)\,^3\Pi_g$ state, the latter state correlating adiabatically to the $5\,^2P_{3/2} + 5\,^2S_{1/2}$ limit. Thus, monitoring the intensity of the atomic $5\,^2P_{3/2} \rightarrow 5\,^2S_{1/2}$ ($D2$) line emission as a function of Δt we obtain real-time traces of the quantum dynamics as viewed through a detection window in the b state.

In practice, the experiments were run in a mildly cooled molecular beam obtained by expanding rubidium vapor at about 700 K through a Ø50 μm nozzle. The molecular beam was intersected by the weakly focused pump and probe pulses of 120 fs duration at a point 4 mm downstream of the nozzle. An interference filter centered at the rubidium $D2$ line served to select the desired fluorescence out of that collected at the right angle to both the molecular and light beams. Saturation effects were checked for and found insignificant and zero delay time was obtained *in situ* by $2 \times \lambda_{pu} + 1 \times \lambda_{pr}$ nonresonant excitation of atomic $7\,^2P \rightarrow 5\,^2S$ fluorescence. For each point Δt in a delay-time scan the fluorescence intensity was measured by gated photon counting averaging over 1000 cycles. The experimental data presented here were obtained by averaging 20 such scans.

The two traces in Fig. 2 were selected out of a set covering pump wavelengths between 865 and 942 nm with $\lambda_{pr} = 1700$ nm. General characteristics of these traces are the well-defined oscillations during the first few picoseconds, the rapid leveling out of the signal at around half the maximum, and the distinct revival structures. The Fourier transform spectra exhibit two main features. First, there is a triplet of regularly spaced bands $\tilde{\nu}_\alpha$, $\tilde{\nu}_\beta$, and $\tilde{\nu}_\gamma$ at 25, 49, and 72 cm^{-1}, respectively, that remains essentially the same in both spectra. This behavior contrasts starkly to that of the $\tilde{\nu}_{b+}$ band at 56 cm^{-1} where intensity is strong with 910 nm pump but weak with 895 nm. Clearly, the 5 ps beat pattern in the former trace corresponds to the $\tilde{\nu}_{b+} - \tilde{\nu}_\beta$ difference frequency, while the indication of a longer beat period 25–30 ps in the upper trace correlates well with the $\sim$1.2 cm^{-1} splitting of the $\tilde{\nu}_\beta$ band.

The most interesting feature of these spectra, we find, is the resonancelike wavelength dependence of the $\tilde{\nu}_{b+}$

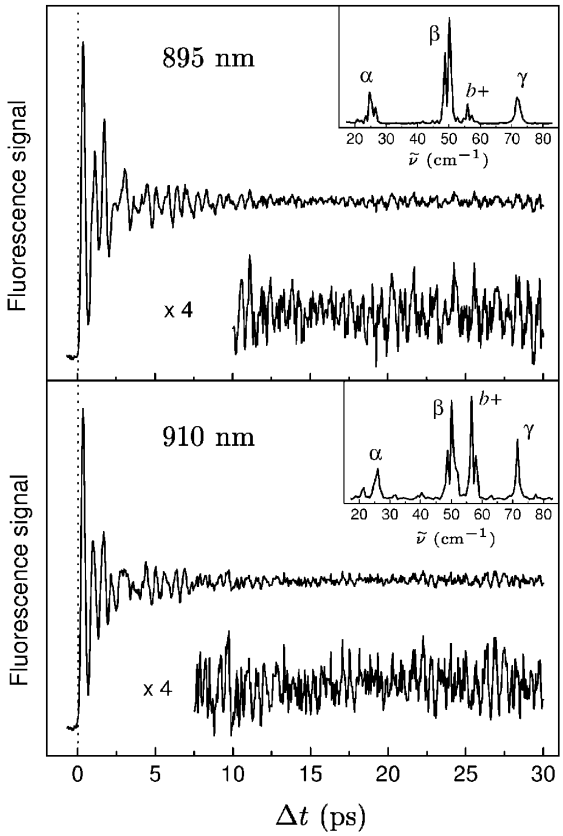

FIG. 2. Measured pump-probe traces and the corresponding fast Fourier transform (FFT) power spectra, defined as $|\mathrm{FFT}|^2$, at indicated pump wavelengths.

band. Before treating that, however, we turn to the $\alpha\beta\gamma$ triplet. The regularity of the triplet indicates that $\tilde{\nu}_\beta$ and $\tilde{\nu}_\gamma$ are approximate overtones of the fundamental frequency $\tilde{\nu}_\alpha$. To see how this might come about, we first note that the pump-probe signal by design is biased towards coherences involving levels of maximally mixed electronic nature, that is, near-degenerate diabatic levels. Such pairs, ignoring for a moment interaction with other diabatic levels, would be split by an average energy $2\langle V\rangle_{T\eta} \approx 2\langle V_{Ab}^{\times} V_v\rangle_{T\eta}$, where V_v is the $A \sim b$ vibrational overlap matrix element and $\langle V\rangle_{T\eta}$ denotes an average of the total coupling element with respect to temperature T and all other parameters η like laser bandwidth, transition probabilities, etc., characterizing the detected density matrix. At a frequency $(\tilde{\nu}_A + \tilde{\nu}_b)/2$ to each side of such a doublet there would be another doublet with less but still considerable degree of mixing and thus similar splitting magnitude.

In general, a level structure as just described does not produce a spectrum consisting of simple harmonics. Would the intrapair splitting be close to half the interpair splitting, however, a spectrum like that of the $\alpha\beta\gamma$ triplet arises with $\tilde{\nu}_\alpha$ corresponding to the intrapair splitting as well as the nearest-neighbor interpair splitting. This is a condition characteristic of the bound-bound intermediate coupling case that seemingly prevails in the present system. Namely, inserting $V_{Ab}^{\times} = 75\ \mathrm{cm}^{-1}$ and a semiclassical estimate $V_v \sim 0.1$–0.2 an expected intradiabatic pair splitting of 15–30 cm^{-1} obtains. Identifying $\tilde{\nu}_\alpha = 25\ \mathrm{cm}^{-1}$ with this splitting and noting that in the crossing region $\tilde{\nu}_A = 44\ \mathrm{cm}^{-1}$ and $\tilde{\nu}_b = 55\ \mathrm{cm}^{-1}$, we see that the simplifying conditions are indeed fulfilled and thus that $\tilde{\nu}_\beta$ and $\tilde{\nu}_\gamma$ may be interpreted as the first two overtones of $\tilde{\nu}_\alpha$. Moreover, the measured spectrum would by this model inherently be stabilized by rotational averaging towards changes in pump wavelength. We accordingly assign the $\alpha\beta\gamma$ triplet to vibrational coherences involving energy levels with this particular intermediate case structure.

Let us now shift attention back to the $\tilde{\nu}_{b+}$ band. In the preceding argumentation we tacitly sidestepped all issues related to the wave packet phase and accompanying interference phenomena. Such phenomena are key factors in understanding longevity resonances in bound-unbound systems [7–11], though, and, in fact, the $\tilde{\nu}_{b+}$ band exhibits the essential features of these resonances: its frequency equals that of motion in an adiabatic state, $\tilde{\nu}_+$, and the strength displays a resonancelike dependence on pump wavelength. This, we propose, is no coincidence and reflects the fact that the mechanism behind the longevity resonances applies also to the bound-bound case with some interesting amendments due to the more complex situation.

Long-lived wave packet resonances in bound-unbound systems arise as follows. An inbound wave packet in the upper, bound state splits at the curve crossing in two fractions continuing along different paths. As the wavelets recur next time at the crossing they may interfere to the extent allowed by overlap and overall phase difference acquired between crossings [16,17]. In the extreme, the dissociative channel closes and all probability density ends up in the original state [9,10]. Would one under such conditions, which are pump wavelength sensitive, probe the wave function at the outer turning point, a signal with a frequency identical to that of the adiabatic state is obtained. Note, however, it is the whole wave packet that is probed. This wave packet is in a well-defined, entangled state of motion consisting of an "adiabatic" wavelet synchronized to a "diabatic" one and can in the intermediate coupling range obviously not be classified according to the diabatic or adiabatic scheme. Instead, for brevity and clarity we shall call such a state mesobatic and label the corresponding entangled wave packet trajectory S_{da}, shown in Fig. 3, by its constituent nominally diabatic (d) and adiabatic (a) paths.

The key to understanding the $\tilde{\nu}_{b+}$ peak, it seems, is to realize that mesobatic conditions may equally well arise in bound-bound systems and that the $\mathrm{Rb}_2(A \sim b)$ case is a likely candidate for this. Namely, in the crossing region $\tilde{\nu}_b \approx \tilde{\nu}_+$ and a slight adjustment in energy of the b potential energy curve suffices to bring about mesobatic wave packet motion, as shown in Fig. 4. Note, in particular, that probing the b part of the wave packet yields a main beat frequency of 57 cm^{-1}, identical within resolution to the experimentally observed $\tilde{\nu}_{b+}$, but also that a different set of harmonics obtains for the A fraction of the same wave packet. As compared to the above, the situation is obviously more complex but the basic mechanism and origin of the $\tilde{\nu}_{b+}$ band in the experiments, we propose, is still dynamical interference.

The comparative complexity of the bound-bound system arises as there exist four potential mesobatic wave packet trajectories, in our case S_{A-}, S_{b+}, S_{A+}, and S_{b-}. These come in pairs, S_{A-}/S_{b+} and S_{A+}/S_{b-}, sharing the

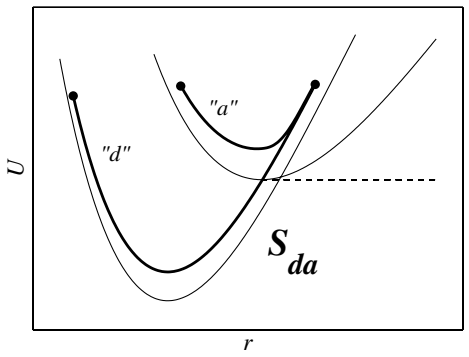

FIG. 3. Mesobatic wave packet trajectory, S_{da} (S_{b+} in the $\mathrm{Rb}_2(A \sim b)$ system), in a bound-bound system when the total acquired quantum phases along the nominal adiabatic a and diabatic d branches, respectively, are the same. If the wave packet is launched in the common turning point of the trajectory, the same motion would appear also in the bound-unbound system indicated by the broken potential curve.

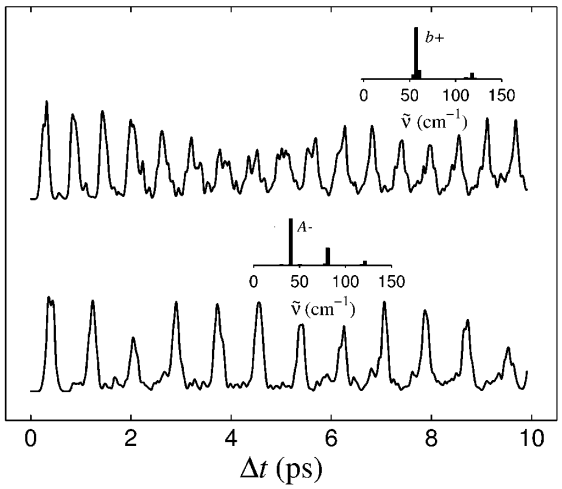

FIG. 4. Calculated quantum dynamical pump-probe traces and the corresponding power spectra for $J = 0$ under mesobatic conditions in the $Rb_2(A \sim b)$ system. An initially Gaussian wave packet at rest at the inner turning point of the A state is propagated [18] and probed at the outer turning point of either the A (lower) or b (upper) state. Other employed parameters correspond to those of the experiments. The potential curves of Ref. [14] were used with a downshift of the b state by 45 cm^{-1} to allow the S_{A-}/S_{b+} pair to meet the mesobatic requirements.

forked part of the trajectories. Interestingly, by an analysis along the lines of Refs. [9,10], it is easily seen that if the mesobatic conditions are met for one pair member then they necessarily apply to the other as well. As a consequence, we need to distinguish two initial conditions for a given mesobatic pair, say S_{A-}/S_{b+}.

To start with, the wave packet may be launched on the common turning point of a mesobatic trajectory. This leads to a situation identical to the predissociation case and the wave packet moves along the initially seeded mesobatic trajectory, S_{A-} or S_{b+}. Another and richer situation arises if the wave packet in our example instead is launched on either of the two inner turning points, e.g., in the A state as in the experiment. At the first encounter with the crossing the wave packet splits in two parts, one continues in the A state while the other swaps to the b state. In the absence of significant interference between the two wavelets at the next crossing, this corresponds to spawning the S_{A-} and S_{b+} trajectories with one wavelet each and for a sufficiently short time they are decoupled. Thus, with a probe window at the outer turning point of the b state we would get a beating of frequency $\tilde{\nu}_{b+}$ while probing at a corresponding location in the A state would yield $\tilde{\nu}_{A-}$, a situation that is recognized in Fig. 4.

In conclusion, we find that the quantum wave packet dynamics in a system of two interacting bound states in the intermediate coupling range consists in general of rapid spreading out over the available classical phase space. There exist particular resonancelike conditions, however, under which the initial wave packet motion is most conveniently described in terms of a coherent superposition of two mesobatic trajectories giving rise to characteristic frequencies at particular pump wavelengths in ultrafast pump-probe spectroscopy. Thermal averaging will reduce the strength of any such features but the characteristic features of the $\tilde{\nu}_{b+}$ band present in Fig. 2 seems to be experimental evidence of a mesobatic state. Having in this short report established their existence, we intend in a forthcoming full paper to elaborate on the properties of the mesobatic wave packet states as well as give more details on the briefly presented experiments and calculations.

We thank Stig Stenholm for discussions on intramolecular quantum interference and the authors of Ref. [14] for providing us with their original data. The work was supported by the Swedish Research Council (VR).

*Electronic address: tony.hansson@physto.se

[1] A. Friedland, Phys. Rev. D **64**, 013008 (2001).
[2] A. Thiel, J. Phys. G **16**, 867 (1990).
[3] M. Larsson, Annu. Rev. Phys. Chem. **48**, 151 (1997).
[4] S. Hahn and G. Stock, J. Phys. Chem. B **104**, 1146 (2000).
[5] M. S. Child, *Semiclassical Mechanics with Molecular Applications* (Clarendon Press, Oxford, 1991).
[6] W. Qin, D. G. McCoy, L. Torop, and A. J. Blake, Chem. Phys. **221**, 77 (1997).
[7] M. J. J. Vrakking, D. M. Villeneuve, and A. Stolow, J. Chem. Phys. **105**, 5647 (1996).
[8] M. Shapiro, M. J. J. Vrakking, and A. Stolow, J. Chem. Phys. **110**, 2465 (1999).
[9] H. Kono and Y. Fujimura, Chem. Phys. Lett. **184**, 497 (1991).
[10] H. Dietz and V. Engel, Chem. Phys. Lett. **255**, 258 (1996).
[11] N. Balakrishnan, B. D. Esry, H. R. Sadeghpour, S. T. Cornett, and M. J. Cavagnero, Phys. Rev. A **60**, 1407 (1999).
[12] M. S. Child, Mol. Phys. **32**, 1495 (1976).
[13] A. N. Hussain and G. Roberts, J. Chem. Phys. **110**, 2474 (1999).
[14] S. J. Park, S.W. Suh, Y. S. Lee, and G.-H. Jeung, J. Mol. Spectrosc. **207**, 129 (2001).
[15] V. Kokoouline, O. Dulieu, and F. Masnou-Seeuws, Phys. Rev. A **62**, 022504 (2000).
[16] B. M. Garraway and S. Stenholm, Phys. Rev. A **46**, 1413 (1992).
[17] G. Granucci and M. Persico, Chem. Phys. Lett. **246**, 228 (1995).
[18] J. Broekhove, B. Feyen, L. Lathouwers, F. Arickx, and P. van Leuven, Chem. Phys. Lett. **174**, 504 (1990).